AJNR

Highlights of the 29th annual meeting of the American Society of Neuroradiology, Washington, DC, June 9-14, 1991.

R N Bryan, J M Caille, D W Chakeres, G DeBrun, W P Dillon, E K Fram, W W Lo, T J Masaryk, M E Mawad and D M Moody

AJNR Am J Neuroradiol 1991, 12 (6) 1241-1249
http://www.ajnr.org/content/12/6/1241.citation

ASNR Section

Highlights of the 29th Annual Meeting of the American Society of Neuroradiology, Washington, DC, June 9–14, 1991

R. Nick Bryan,[1] Jean Marie Caille,[2] Donald W. Chakeres,[3] Gerard DeBrun,[1] William P. Dillon,[4] Evan K. Fram,[5] William W. M. Lo,[6] Thomas J. Masaryk,[7] Michel E. Mawad,[8] Dixon M. Moody,[9] Ruth G. Ramsey,[10] Hervey D. Segall,[11] Wendy R. K. Smoker,[12] Gordon K. Sze,[13] Anton G. Valavanis,[14] Alan L. Williams,[15] and Robert D. Zimmerman[16]

A special focus session on pediatric neuroradiology began the 29th annual meeting of the American Society of Neuroradiology in Washington, DC, held on June 9–14, 1991. Six more special focus sessions, 44 technical exhibits, 225 paper presentations, 65 scientific exhibits, 60 posters, and 48 excerpta extraordinaire incorporated new topics in the field of neuroradiology with improvements to existing methods of treatment and diagnosis. This report summarizes some of the significant points from the scientific presentations.

Pediatric Neuroradiology

The special focus session on pediatric neuroradiology was followed by paper 1 by Stark et al., describing combined-method imaging with contrast-enhanced CT and sonography in cases of retropharyngeal abscess in children. Sonography was particularly useful in differentiating retropharyngeal abscess from cellulitis. High-dose chloral hydrate as a safe and effective sedative for children undergoing MR and CT was the subject of paper 2 by Patel et al., in which the authors administered a dose of 100–150 mg/kg with an overall success rate of 96%, a "mild" complication rate of 13%, and no major complications. Chloral hydrate was found to be much more effective in sedating children when higher-than-standard doses are used. However, the top suggested dose of 150 mg/kg exceeds the maximum dose (120 mg/kg) recommended in the American Academy of Pediatrics Guidelines.

[1] The Johns Hopkins Hospital, Baltimore, MD 21205.
[2] Hospital Pellegrin, Cedex, Bordeaux, 33076, France.
[3] Ohio State University Hospital, Columbus, OH 43210.
[4] UCSF Medical Center, San Francisco, CA 94143.
[5] Barrow Neurological Institute, Phoenix, AZ 85013.
[6] St. Vincent Radiological Medical Group, Los Angeles, CA 90057.
[7] The Cleveland Clinic Foundation, Cleveland, OH 44195-5103.
[8] The Methodist Hospital, Houston, TX 77030.
[9] Bowman Gray School of Medicine, Winston-Salem, NC 27103.
[10] University of Chicago, Chicago, IL 60637.
[11] USC School of Medicine, Los Angeles, CA 90033.
[12] Medical College of Virginia, Richmond, VA 23298.
[13] Yale Medical Center, New Haven, CT 06510.
[14] Universitatsspital Zurich, Zurich, CH-8091, Switzerland.
[15] Froedtert Memorial Lutheran Hospital, Milwaukee, WI 53226.
[16] New York Hospital, New York, NY 10021.

AJNR **12:1241–1249, November/December 1991** 0195–6108/91/1206–1241

Klucznik et al. (paper 4) reported on spoiled GRASS MR imaging in children. This pulse sequence appears to provide excellent gray-white matter differentiation and appreciates signal changes related to the myelination process earlier than standard T2-weighted imaging. Jouandet et al. (paper 6) described a novel approach to mapping of the cerebral hemispheres with great potential for the direct comparison of physiologic and anatomic data. Figueroa et al. (paper 7) reported proximal major vessel disease in patients with sickle cell vasculopathy, particularly stenosis of the supraclinoid internal carotid artery (Fig. 1). Sickle cell disease was also the subject of a paper by Smith et al. (paper 8), who reported good correlation between MR/MR angiography abnormalities and clinical symptoms.

A comparison by Boyko et al. (paper 11) of quantitative volumetric MR findings found in patients with periventricular leukoencephalopathy and spastic diplegia and in a normal control population demonstrated a practical method for volumetric quantitation from hard-copy films. This method shows promise as an alternative to computerized 3-D imaging and it takes only about 20 min to perform. Paper 12 by Valk et al. pointed out the complexity of hypoxic-ischemic injury in neonates. Many factors are involved, including myelination, vascular supply, and changing neurochemistry. Several patterns of injury may result from various combinations of these factors. The authors conclude that MR has a place in the early diagnosis and follow-up of preterm neonates with hypoxic-ischemic injuries, such as subiculum necrosis (Fig. 2). MR of infarction in neonates and infants is not obvious, and is seen as isointensity of cortex and underlying white matter. Papers 13 (Lindan and Barfouica) and 16 (Heier) pointed out the extreme subtlety of these findings on MR images obtained in the first 48 hr after injury. CT may be the method of choice for detecting hypoxic-ischemic injury in the neonatal period. Armstrong et al. (paper 14) showed that posttraumatic and mycotic aneurysms constitute a greater proportion of aneurysms in children than in adults.

Spine Imaging

Dynamic turboflash imaging of the cervical spine reported by Schnapf et al. (paper 17) was found to be useful in acute cervical spine trauma and other spinal diseases, including herniated disks. Greiner et al. (paper 18) advocated vertebral angiography in cervical spine fracture/subluxation. Half of their patients showed some vertebral artery abnormality, including complete occlusion, intimal flap, and/or spasm. Sze et al. (paper 20) evaluated phased array coils for multilevel spinal MR imaging, indicating improvement in signal-noise ratio and field of view over conventional techniques. This could be advantageous for evaluations of spinal cord compression and metastatic disease. Preliminary experience with hybrid T2-weighted sequences in the spine indicates advantages in the detection of intra- and extradural disease (Merriam et al., paper 21). These sequences have true T2 contrast and less susceptibility artifact than do gradient-echo studies and they also have shorter scan times with less motion degradation compared with conventional T2-weighted spin-echo sequences. Contrast-enhanced MR imaging was shown to be a sensitive diagnostic method for detecting spinal dural arteriovenous fistulas (Gray et al., paper 30). MR imaging was reported by Jordan et al. (paper 25) to be more cost effective than myelography in the work-up of patients with documented cord compression.

Neoplasms

The Cornelius G. Dyke Award paper dealt with the quantitation of pathologic blood-brain-barrier permeability in a rat astrocytic glioma model using contrast-enhanced MR imaging. The award winner, U. P. Schmiedl (U. Washington, Seattle), related size of contrast molecule to the degree of enhancement.

Forsting et al. (paper 32) discussed the prognostic value of baseline CT and MR after malignant brain tumor resection. They found MR superior in documenting postoperative tumor resection. A report on the use of computerized imaging and image processing by Kikinis et al. (paper 33) demonstrated the value of 3-D reconstructed images in neurosurgical planning. Figure 3 demonstrates a protoplasmic astrocytoma, a typically superficial, nonenhancing glioma that is relatively benign, as reported by Eisenberg and Norman (paper 38). Surgical and pathologic correlations of MR images of menin-

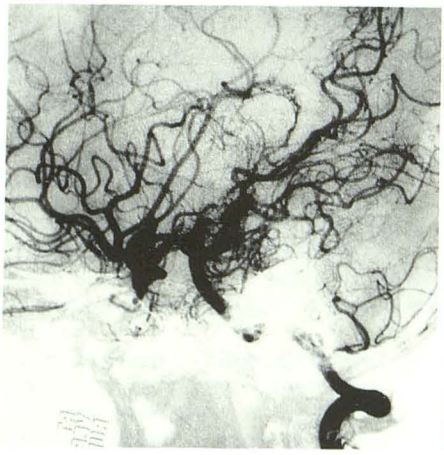

1

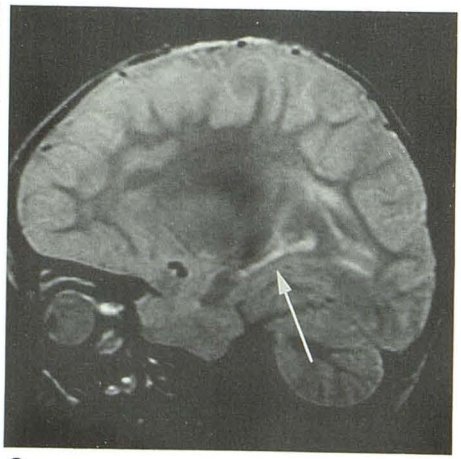

2

Fig. 1.—Sickle cell disease. Lateral view of vertebral arteriogram shows collateral circulation to carotid circulation distal to supraclinoid internal carotid occlusion.

Fig. 2.—Subiculum necrosis. T2-weighted MR image shows increased signal intensity in subiculum (*arrow*) after neonatal ischemia.

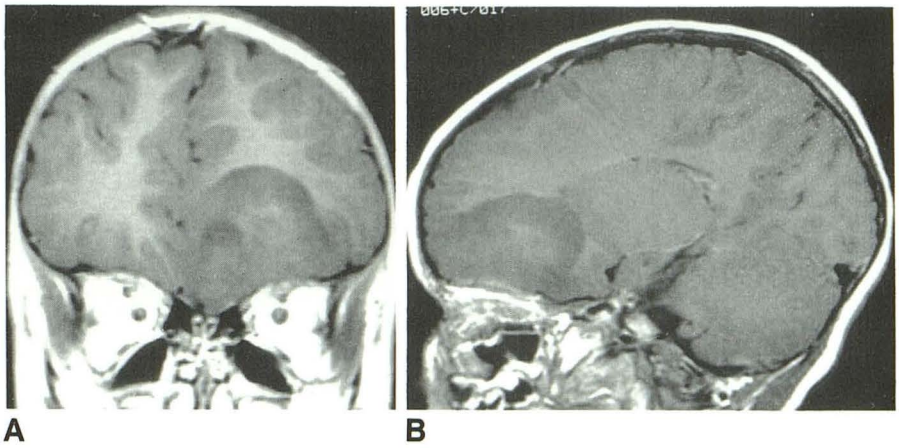

Fig. 3.—Frontal protoplasmic astrocytoma. Coronal (*A*) and parasagittal (*B*) T1-weighted MR images show a typical, superficial, well-delineated mass.

giomas revealed that hyperintensity on T2-weighted images has a high correlation with soft-tumor consistency at surgery and also suggests aggressive histopathology. Hypointensity in nonhemorrhagic tumors on T2-weighted images was indicative of benign histopathology in a study by Zee et al. (paper 61). The MR appearance of dysembryoplastic neuroepithelial tumors was explored by Koeller (paper 63). These are benign neoplasms arising within the cortex of the cerebral hemispheres, usually associated with seizures. MR demonstrated a focal cortical mass in the six patients studied. Robles et al. (paper 65) summarized the appearance of 49 primitive neuroectodermal tumors and noted that these tumors elicited little reactive edema and became more complex and heterogeneous as they became larger (Fig. 4).

Inflammation/AIDS

Eisenberg et al. (paper 68) confirmed that toxoplasmosis and lymphoma are the most common basal ganglia lesions in AIDS patients (nine of their 13 cases). The rest of their patients had cryptococcosis, atypical TB, or neurosyphilis (Fig. 5). A prospective evaluation of the utility of gadopentetate dimeglumine in HIV-positive patients with suspected CNS disease was presented by Gean-Marton et al. (paper 69). The authors concluded that by limiting the use of contrast agent to a selected subset of patients, quality of care can be preserved while limiting cost, examination time and the risk of needle sticks. Hemorrhagic CNS lesions and their mimics in patients with AIDS were the subject of study by Destian et al. (paper 70). Detailed clinical and pathologic correlations were made with MR imaging in 10 patients with AIDS believed to have hemorrhagic lesions by MR. Three hemorrhaged into existing lesions (two toxoplasmosis, one lymphoma). Two hemorrhages were iatrogenic (stereotaxic biopsy). The remaining patients had high signal lesions on T1-weighted images that did not represent hemorrhage. It is not yet certain to what extent the presence of necrotic debris, gliosis, occluded vessels, and/or lipid-laden macrophages may have contributed to the observed hyperintensity.

A study of the natural history of multiple sclerosis (MS) involving 156 monthly MR scans of 11 MS patients demonstrated that 87% of the patients had reenhancing lesions (Armstrong et al., paper 77). They also noted an approximately 7-month recycling time of lesion enhancement in these untreated patients. Simon et al. (paper 87) discussed computer-assisted analysis in cerebral MS by using a method of measuring plaques volumetrically on both T2- and contrast-enhanced T1-weighted images. These methods will probably become increasingly important in the future and will supplant traditional ways of comparing plaques on similar axial sections of different studies in order to follow the progress of MS.

Trauma and Hemorrhage

Weingarten et al. (paper 84) noted that while MR was not as sensitive to diffuse subarachnoid hemorrhage as CT, focal clots can be well demonstrated. Of particular note are small clots in the area of the basilar artery tip that were associated with normal angiographic findings in six of eight cases (Fig. 6). Zimmerman et al. (paper 88) described a potentially useful technical innovation. In a spiral tomography unit, the gantry continually rotates and acquires X-ray attenuation data while the table moves the patient smoothly through the gantry with an uninterrupted motion. Advantages include speed (12–24 sec) of examination time and more intense opacification of the vasculature in an infusion study. It is believed that this unit will be useful in the evaluation of CNS emergencies in children.

Two papers dealt with superficial hemosiderosis (paper 91 by Jahre et al. and paper 92 by Triulzi et al.). This condition is easily identified by the striking appearance of low signal on the brain surface in T2-weighted images (Fig. 7). This condition by itself can be asymptomatic or it may be etiologically important in the development of deafness, cerebellar ataxia, and dementia, which are sometimes found in these patients. T2-weighted and gradient-echo images best demonstrate the hemosiderosis around the basal cisterns and in the cerebellar folia; the high convexities are often spared.

Davenport and Sze (paper 98) compared hybrid T2-weighted fast spin-echo sequences with conventional T2-weighted spin-echo sequences in cranial MR imaging. The hybrid T2-weighted images were acquired in less time and represent an alternative to long TR spin-echo imaging.

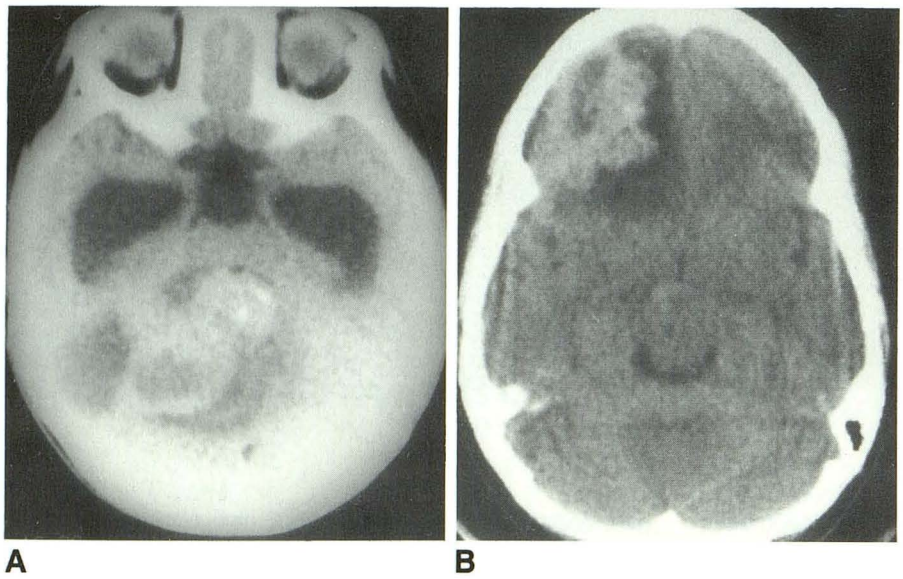

Fig. 4.—Primitive neuroectodermal tumors (PNET). Unenhanced CT scans of large infratentorial (*A*) and supratentorial (*B*) PNET with characteristic heterogeneous appearance.

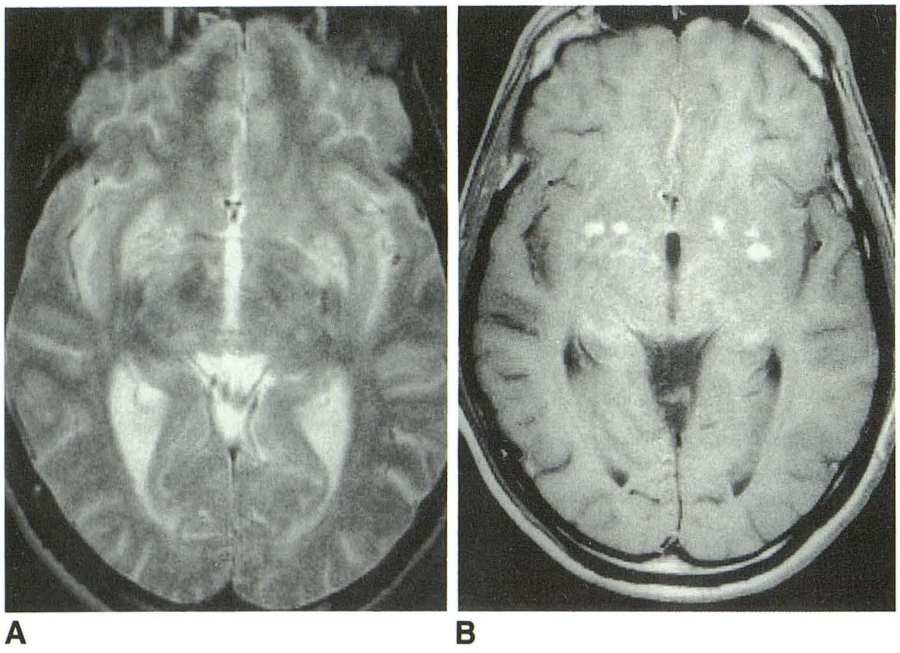

Fig. 5.—Neurosyphilis. T2-weighted (*A*) and postcontrast T1-weighted (*B*) MR images of AIDS patient with basal ganglia neurosyphilis.

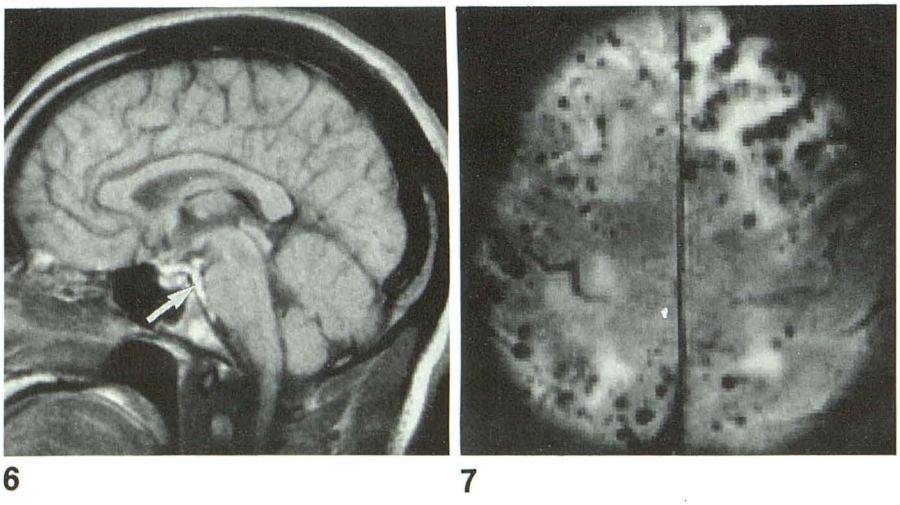

Fig. 6.—Focal subarachnoid hemorrhage. Sagittal T1-weighted MR image shows prepontine hemorrhagic signal (*arrow*) in a patient with normal findings on cerebral angiography.

Fig. 7.—Superficial hemosiderosis. T2-weighted MR image shows diffuse and punctate low-signal regions in patient following subarachnoid hemorrhage.

Stroke

It is well known that there is a significant risk of neurologic or neuropsychologic deficits following cardiac surgery assisted by cardiopulmonary bypass (CPB).Two excellent papers reported the possible etiology and the application of MR in the detection of related brain injury. Moody and colleagues (paper 100) prospectively studied brain specimens in subjects with recent CPB (eight humans, six dogs) and those without CPB (38 humans, six dogs). They found small capillary/arterial dilatations (SCADs) in every subject with recent CPB, several million in some cases, but not in any of the brains without CPB. They believed the SCADs represent the "footprint" of the site formerly occupied by microemboli of approximately 10–50 μm in size. Brain injury related to CPB was further evaluated by MR imaging by DeLaPaz and co-workers (paper 101). They prospectively studied 26 patients with recent CPB for cardiac valve-replacement surgery by comparing their pre- and postsurgical noncontrast MR studies. Fifteen patients (58%) developed new lesions identified as high-signal abnormalities on T2-weighted spin-echo images. Most of these patients (eight of 26, 31%) had lesions that were small (2–5 mm), periventricular white matter and corpus callosum abnormalities most consistent with white matter ischemia. The remainder (seven of 26, 27%) had focal lesions, probably infarcts, in the brainstem, cerebellum, basal ganglia, and cerebral hemispheres. The cause of the new MR lesions was most likely embolism, especially the focal infarctions, but in several cases the new white matter abnormalities were clustered in the centrum semiovale and suggested watershed ischemia as the cause.

Major issues regarding the intravascular thrombolytic treatment of acute ischemic stroke remain controversial. The optimal dose of IV tPA treatment within the first 6 hr was not determined by Wolpert (paper 103) in his dose-escalating study of 92 patients from 13 medical centers or by von Kummer and colleagues (paper 106) in their study of 24 patients. In these two studies, recanalization occurred in 34–41% and bleeding complications in 19–34%. Wolpert and von Kummer and associates noted that recanalization was achieved more frequently in branch or distal cerebral occlusion than in carotid or main stem middle cerebral artery occlusion. The size of the infarction did not increase in patients with bleeding complications. Von Kummer and co-workers emphasized that good collateral circulation, demonstrated on the initial pretreatment angiogram, and evidence of recanalization, even 24 hr after stroke, are important preconditions for a favorable clinical outcome. Intraarterial thrombolytic therapy appeared to have a better recanalization rate in occlusions involving larger blood vessels and a much lower rate of bleeding complications (patient number/recanalization rate/bleeding rate: 6/66%/17%) as reported by Nakahara and collaborators (paper 102) and by Picard and colleagues (7/43%/0%) (paper 104). On the basis of the presented data it appeared that IV tPA may be more successful in the treatment of occlusions in smaller vessels whereas intraarterial thrombolytic treatment may be more effective in the treatment of occlusions in large vessels. Bleeding complications decrease with early and/or intraarterial treatments.

Mueller and associates (paper 110) reported that abnormal arterial enhancement (AE) observed in acute ischemic stroke is caused by slow arterial flow. They compared the MR findings with angiograms obtained within 24 hr of the MR examination in 16 patients and found that AE was not always associated with angiographic evidence of occlusion. In the patients with AE, all but one were symptomatic (with or without occlusion) and most had angiographic evidence of slow flow. All patients without AE were asymptomatic (with or without occlusion) and did not have angiographic evidence of slow flow. They concluded that the presence of AE is an indicator of slowed (diminished) cerebrovascular circulation and appears to correlate with clinical status.

Head and Neck Imaging

Levy et al. (paper 117) demonstrated that a combination of appropriate (coronal) CT scans and 3-D computer technology can accurately delineate and optimally display facial fractures (Fig. 8). Mark et al. (paper 119) studied the clinical and pathologic correlation of contrast-enhanced MR imaging in enhancement of the cisternal segment of the third nerve. The authors concluded that MR may provide positive imaging correlation in patients whose diagnosis in the past was one of clinical exclusion, such as Tolosa-Hunt syndrome and ophthalmoplegic migraine. Papers 121 and 123 (Mawad et al. and Mintz et al.) provided a good discussion of imaging and anatomy of nontumorous enlargement of the optic nerve and a comparison of MR vs sonography in the evaluation of ocular melanoma, respectively.

Vascular Disease

From an angiographic population of 1456, three examples of proximal vertebral artery dissections were found by Friedman and Flanders (paper 201) (Fig. 9). The MR characteristics of clinical hemorrhage in cerebral arteriovenous malformations were studied by Chappell et al. (paper 205). MR was found to be accurate in defining those patients who had evidence of prior bleeding episodes. Gradient-recalled-echo images were more sensitive than spin-echo images in identifying hemosiderin deposition. Central venous drainage, paraventricular location, and intranidus aneurysms were all visible on MR and correlated well with high-risk lesions. Arteriovenous malformations (AVMs) were also the subject of study by Carbonneau et al. (paper 206). Findings from five patients with pial or dural AVMs were discussed. All the patients had extensive adjacent brain edema, and all had evidence of venous thrombosis or obstruction. Recognition of these tumorlike AVMs is important and requires special consideration prior to diagnostic procedures and therapy. The importance of angiography in micro AVMs was emphasized by Willinsky et al. (paper 207), who found that CT, MR, and even acute posthemorrhage angiography missed a significant number of these lesions (Fig. 10).

New observations on the association of venous angioma, hemorrhage, and cryptic vascular malformations were offered by Dillon et al. (paper 208). Patients with acute or subacute cerebrovascular hemorrhages were examined. The reported patients had venous angiomas in conjunction with a cryptic

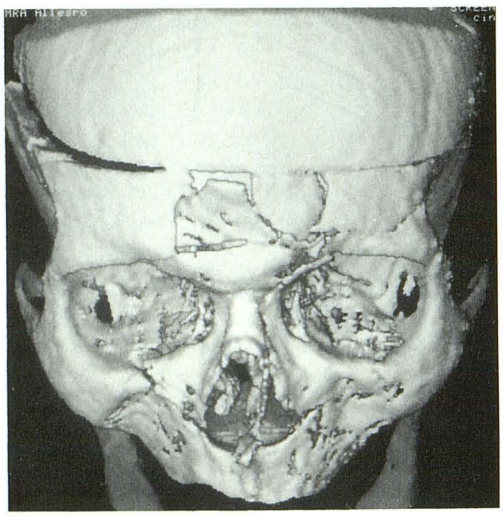

Fig. 8.—Phantom facial fractures. 3-D reconstruction of coronal CT scans of skull with engineered fractures simulating common clinical fractures.

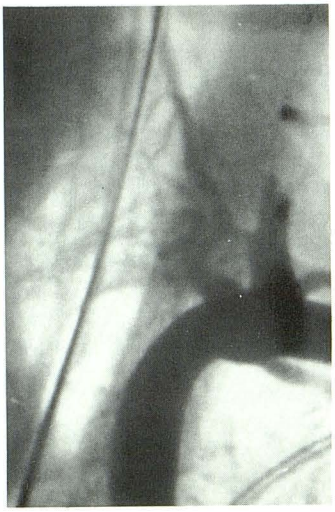

Fig. 9.—Dissection of vertebral artery. Anteroposterior view of left subclavian angiogram with dissection at origin of vessel.

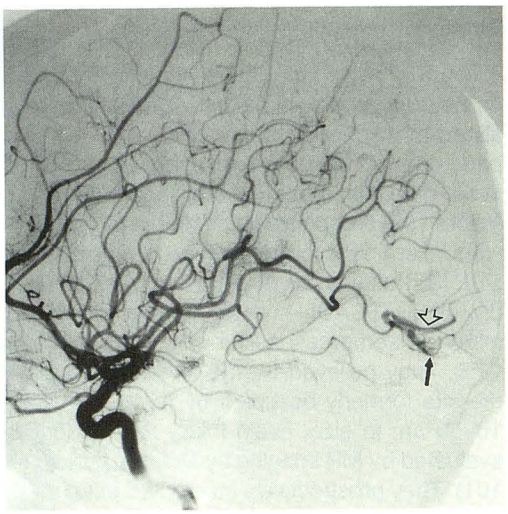

Fig. 10.—Micro AVM. Lateral carotid angiogram shows lesion (*closed arrow*) with its early draining vein (*open arrow*).

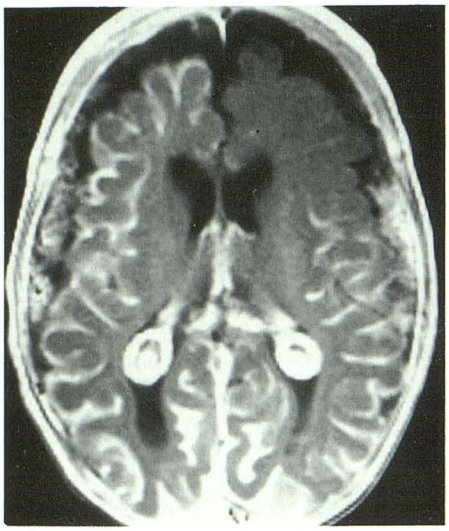

11

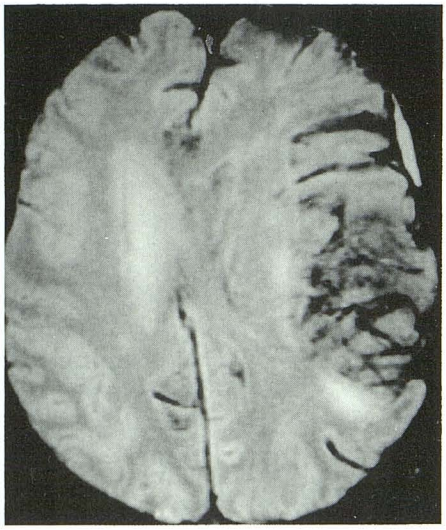

12

Fig. 11.—Sturge-Weber syndrome. Bilateral pial enhancement on postcontrast T1-weighted MR image.

Fig. 12.—Subarachnoid hemorrhage. Gradient-echo (500, 30,15°) image shows low signal in left cerebral sulci from acute subarachnoid hemorrhage.

arteriovenous malformation or hemorrhage. These patients also had evidence of stenosis of the venous angioma. This may in part account for the increased frequency of hemorrhage and may be the cause of hemorrhagic complications associated with venous angiomas. Marks et al. (paper 209) evaluated intracerebral AVMs by using phase-contrast cine MR techniques to estimate cerebral blood flow via the major arterial supply to the brain. The authors demonstrated elevated flow rates and velocities of all major arteries in patients with AVMs. Ipsilateral flow to the side of the AVM was most pronounced. The technique shows promise for use in following patients with AVMs who are at risk for steal symptoms or normal perfusion breakthrough bleeding.

Interventional Neuroradiology

A comparison of Silastic and latex balloons for endovascular treatment of a rabbit model of cerebral aneurysm was performed by Kwan et al. (paper 198), who found that there was a greater degree of aneurysm closure with the latex balloons, probably because they evoked more reactive fibrosis. Paper 199 by Mehta et al. demonstrated the use of a new polymer (Hydrogel) stent that was used to close aortocaval fistulae that had been created in rats. Three cases of acute superior sagittal sinus thrombosis successfully treated with direct endovascular urokinase thrombolysis were presented by Tsai et al. (paper 217). Zenteno et al. (paper 220)

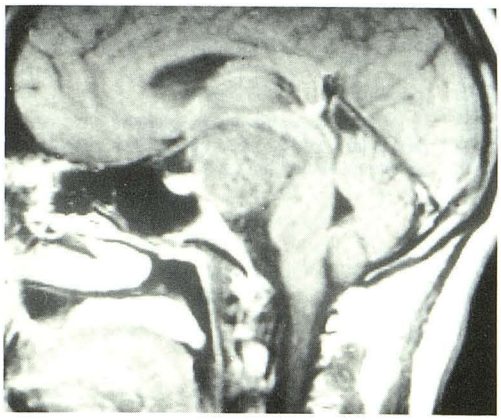

Fig. 13.—Intradural chordoma. Sagittal T1-weighted MR image with postclival mass.

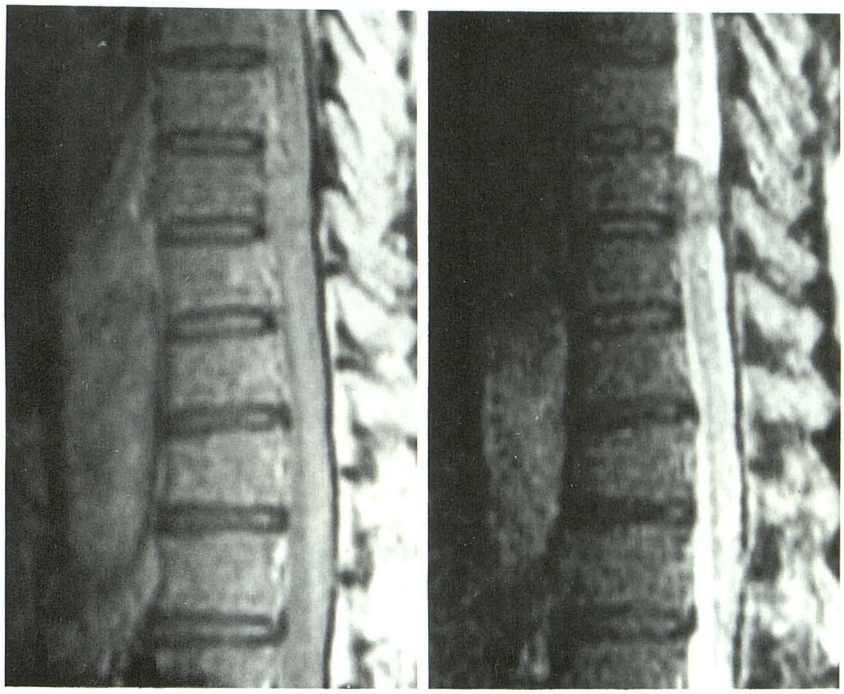

Fig. 14.—Leiomyoma of vertebral body. Proton-density-weighted (*left*) and T2-weighted (*right*) MR images show lesion with signal that is isointense with muscle.

Fig. 15.—Extramedullary hematopoiesis (*arrows*).

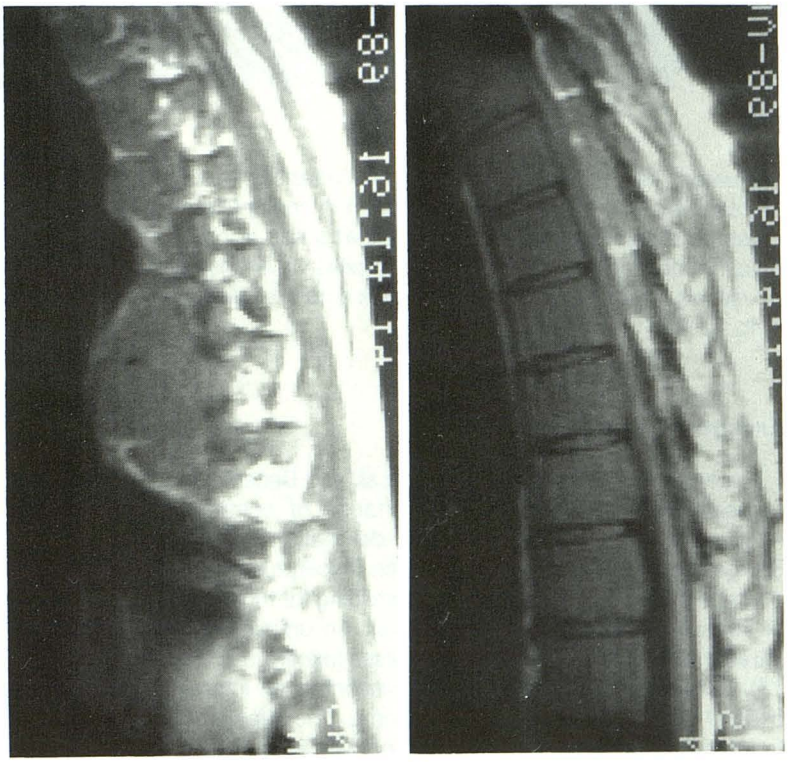

A B

Fig. 16.—Extramedullary hematopoiesis. Parasagittal (*A*) and sagittal (*B*) T1-weighted MR images show paraspinal mass with posterior extension and epidural mass.

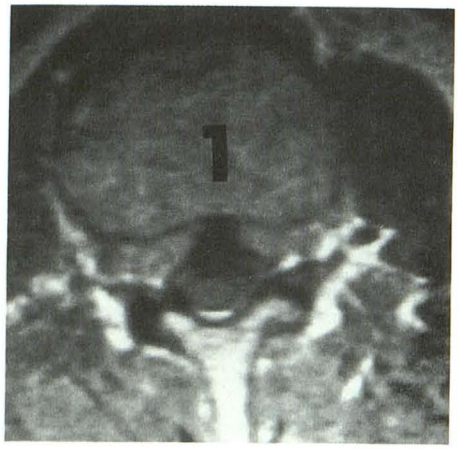

17

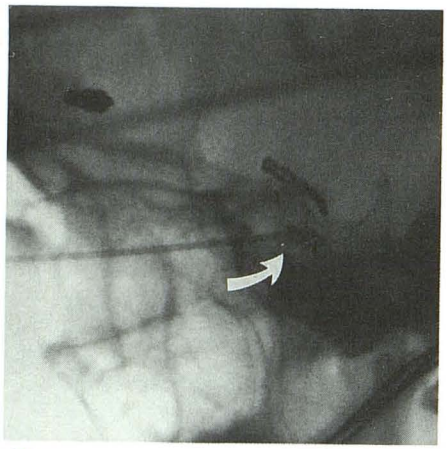

18

Fig. 17.—Herniated disk. T1-weighted MR image shows acute, "butterfly" herniated disk tethered centrally by posterior longitudinal ligament.

Fig. 18.—Carotid cavernous fistula (CCF). *Arrow* points to Gianturco coil placed in CCF via paranasal sinus approach.

19

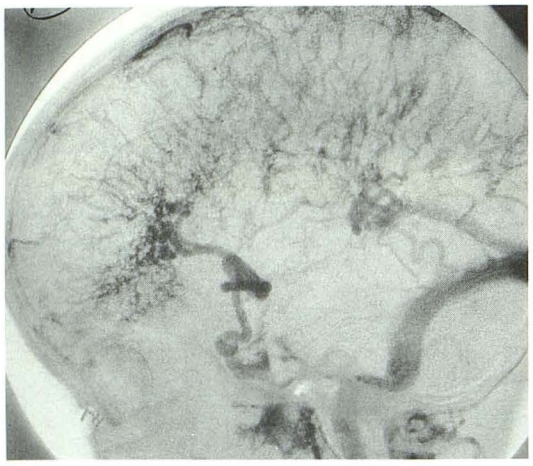

20

Fig. 19.—Venous angiomas. Bilateral cerebellar venous angiomas as seen on MR angiography.

Fig. 20.—Giant venous angioma. Lateral, venous phase, carotid angiogram of venous angioma involving most of the venous drainage of a cerebral hemisphere.

evaluated the predictive value of AVM intrapedicle sodium amobarbitol (Amytal) injection performed in conjunction with pressure recordings. They proposed that a rise in pressure measurements after Amytal injection implies vasoconstriction of vessels supplying normal brain and is a contraindication to embolization at that point.

Excerpta Extraordinaire

Excerpta 9 and 10 by O'Sullivan et al. and Benedict et al., respectively, emphasized the importance of contrast enhancement for the diagnosis and delineation of atypical Sturge-Weber disease (Fig. 11). Olsen (excerptum 14) demonstrated the value of gradient-echo imaging for the detection of subarachnoid hemorrhage (Fig. 12). An unusual case of intradural chordoma was shown by Olsen (excerptum 15, Fig. 13). Excerptum 27 (Knopp et al.) presented an interesting case of primary cauda equina lymphoma. The affected, matted nerve roots were not identified on MR scans but were well-appreciated on CT myelography. An interesting case of vertebral body leiomyoma at T9 was shown by Walot et al. (excerptum 28). The tumor signal intensity paralleled that of muscle on proton-density-, T1-, and T2-weighted images (Fig. 14). Excerpta 29 (Kalina) and 30 (Choi et al.) presented three patients with thalassemia-related extramedullary hematopoiesis and resulting spinal cord compression imaged by MR. Hypointensity of vertebral bodies with an expanding, enhancing epidural mass was demonstrated (Figs. 15 and 16). Excerptum 32 by Carbonneau and Oot demonstrated an unusual, acute "butterfly" herniated disk (Fig. 17). Hoffman et al. (excerptum 33) presented two cases of the rare split notochord syndrome with dorsal enteric fistula. The association of bladder extrophy and imperforate anus (OEIS) in one patient raises the possibility of an association between the split notochord syndrome and the OEIS complex. Excerptum 37 by Chin et al. is a case report of a 24-year old woman with left direct carotid cavernous fistula (CCF) and traumatic occlusion of the left internal carotid artery sustained in a motor vehicle accident. The CCF was refractory to supraclinoid carotid occlusion and subsequent endovascular therapy. The CCF was occluded by using a direct approach to the cavernous sinus through the ethmoid and sphenoid sinuses by means of fluoroscopically guided puncture and placement of Gianturco coils—a unique approach and solution to a difficult clinical problem (Fig. 18). Two excerpta, one by Wesolowski

et al. (excerptum 39) and the other by Dawson and Horton (excerptum 40) addressed unusual venous angiomas. The first showed bilateral cerebellar lesions on MR angiography (Fig. 19) while the second showed a giant angioma involving an entire cerebral hemisphere (Fig. 20). Excerptum 41, presented by Brothers et al., was a report of two patients with intramedullary spinal cord AVMs who underwent test occlusion of the ascending limb of the artery of Adamkiewicz to assess adequacy of collateral supply to the anterior spinal artery prior to surgical resection. Both had surgical occlusion of the anterior spinal artery at the AVM without neurologic consequences. The test occlusion provided key information that increased confidence during surgery, a natural extension of internal carotid artery test occlusion.

Excerptum 44 by Eskridge et al. described a patient with superior sagittal sinus thrombosis (SSS) treated with direct transcatheter infusion of urokinase into the SSS by way of a transfemoral and transjugular approach. Infusion was carried out over 36 hr. Five days later the patient had regained consciousness and was neurologically normal. This is an exciting technique that will probably become more common in the future.